Logarithmic Entanglement Growth from Disorder-Free Localization in the Two-Leg Compass Ladder

Oliver Hart,[1] Sarang Gopalakrishnan,[2,3,4] and Claudio Castelnovo[1]
[1]*T.C.M. Group, Cavendish Laboratory, JJ Thomson Avenue, Cambridge CB3 0HE, United Kingdom*
[2]*Physics Program and Initiative for the Theoretical Sciences, Graduate Center, CUNY, New York, New York 10016, USA*
[3]*Physics and Astronomy, College of Staten Island, Staten Island, New York 10314, USA*
[4]*Department of Physics, The Pennsylvania State University, University Park, Pennsylvania 16802, USA*

(Received 25 September 2020; accepted 11 March 2021; published 4 June 2021)

We explore the finite-temperature dynamics of the quasi-1D orbital compass and plaquette Ising models. We map these systems onto a model of free fermions coupled to strictly localized spin-1/2 degrees of freedom. At finite temperature, the localized degrees of freedom act as emergent disorder and localize the fermions. Although the model can be analyzed using free-fermion techniques, it has dynamical signatures in common with typical many-body localized systems: Starting from generic initial states, entanglement grows logarithmically; in addition, equilibrium dynamical correlation functions decay with an exponent that varies continuously with temperature and model parameters. These quasi-1D models offer an experimentally realizable setting in which natural dynamical probes show signatures of disorder-free many-body localization.

DOI: 10.1103/PhysRevLett.126.227202

Introduction.—The far-from-equilibrium dynamics of isolated many-body quantum systems has been a very active topic of research in multiple fields of contemporary physics, ranging from decoherence in quantum information theory to the black hole information paradox [1–3]. A central topic in this field has been the phenomenon of "many-body localization" (MBL), by which an isolated quantum system fails to reach a local equilibrium state starting from generic initial conditions [4–7]. In systems subject to strong quenched randomness, the existence of MBL can be proven under minimal assumptions [8]. Whether MBL can happen in systems with (discrete) translation invariance is a relatively subtle question [9–14]: in fully generic systems of this kind, it seems likely that strict MBL (i.e., a regime where a system never approaches equilibrium) is impossible [15,16], at least in the conventional thermodynamic limit [17]. However, in many specific (albeit fine-tuned) models, disorder-free localization can be established; near these fine-tuned limits, one expects the phenomenon to persist to long times, though perhaps not asymptotically [18–25].

Experimental studies of MBL have, hitherto, been conducted mostly on cold-atom systems and other forms of synthetic quantum matter [26–32] (apart from a few studies on disordered semiconductors and superconductors [33–36], and a very recent study on phonons [37]). The key condition for disorder-free localization—namely, the presence of local conserved charges that generate intrinsic randomness at finite temperature—can also be satisfied in strongly correlated electronic systems. However, studies of disorder-free localization in this setting have, so far, focused on somewhat fine-tuned models that are of limited experimental relevance and on operators that are diagonal in the conserved charges.

Here, we study specific spin ladder models that are relevant to the description of transition metal oxides [38], with an emphasis on quantities that can be measured in experiment, such as the dynamical structure factor. The models under consideration may be mapped to free fermions coupled to emergent disorder provided by local $\mathbb{Z}_2$ conserved charges. In contrast to previous studies, we are primarily interested in the behavior of operators or quantities that modify the emergent disorder realization. Such sector-changing operators are unique to systems in which the disorder is emergent, and thus the phenomenology that we consider goes beyond that of systems where the disorder is quenched. Specifically, we explore the growth of entanglement and the dynamical response of these models by relating them to Loschmidt echoes in free-fermion systems [23]. These free-fermion methods give us access to much larger system sizes than are usual in the study of MBL. Our main result is that both the entanglement dynamics and the experimentally relevant response properties of these models follow the predictions for generic many-body localization: entanglement grows logarithmically in time [39–44], and certain dynamical correlation functions decay with anomalous power laws [45–49]. Given that the model is essentially noninteracting, this behavior is surprising. Beyond being experimentally relevant in the study of strongly correlated materials [38], our models afford us a level of analytical understanding that allows us to elucidate why disorder-free single particle

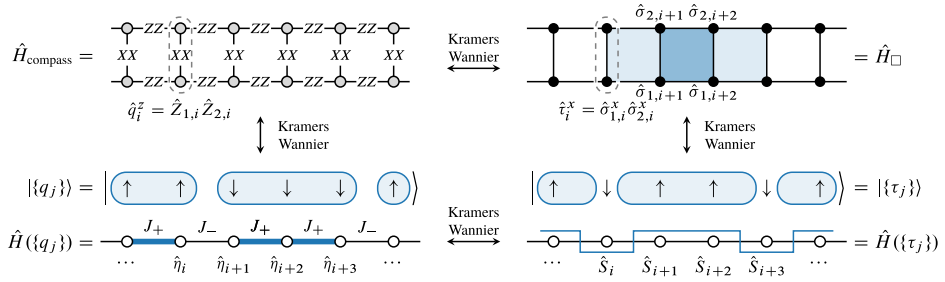

FIG. 1. Schematic depiction of the model and its mapping to a disordered transverse field Ising model. A Kramers-Wannier duality of the compass model (1) along the rungs isolates the conserved charges $\hat{q}_i^z = \hat{Z}_{1,i}\hat{Z}_{2,i}$. Within each charge sector $\{q_j\}$, the Hamiltonian of the $\hat{\eta}$ spins $\hat{H}(\{q_j\})$ corresponds to an Ising model with nearest neighbor coupling $J_{i,i+1} = \Gamma_1 + \Gamma_2 q_i q_{i+1}$. The compass model (1) is also dual to the plaquette-Ising model (3) via a standard Kramers-Wannier transformation.

localization due to emergent randomness can give rise to the same phenomenology as MBL.

We focus our attention on the square lattice compass model [38,50,51], which may be viewed as a quasi-one-dimensional analogue of the Kitaev honeycomb model [52]. This model is dual to the plaquette Ising model [53,54], which has been explored as a prototypical model with "fractonlike" excitations, i.e., excitations whose motion is confined to reduced dimensions [55]. The relation between fractons and disorder-free MBL also remains largely unexplored in the literature (but see Ref. [56]).

Models and mappings.—We begin by introducing the compass model on a two-leg ladder [38], as illustrated in Fig. 1

$$\hat{H}_{\text{compass}} = -\Delta \sum_{j=1}^{L} \hat{X}_{1,j}\hat{X}_{2,j} - \sum_{j=1}^{L-1}\sum_{\alpha=1}^{2} \Gamma_\alpha \hat{Z}_{\alpha,j}\hat{Z}_{\alpha,j+1}, \qquad (1)$$

where $(\hat{X}_{\alpha,j}, \hat{Z}_{\alpha,j})$ are the usual Pauli matrices on leg $\alpha = 1, 2$ and rung $j = 1, \ldots, L$. Introducing the operators $\hat{q}_j^z = \hat{Z}_{1,j}\hat{Z}_{2,j}$ on each rung, $[\hat{H}, \hat{q}_j^z] = 0$ since the operators $\hat{q}_j^z$ and $\hat{X}_{1,j}\hat{X}_{2,j}$ share either zero or two sites. This leads to an extensive number of conserved charges $\{q_j\}$, one for each rung of the ladder; since $(\hat{q}_j^z)^2 = \mathbb{1}$, the conserved c numbers are $q_j = \pm 1$. The conserved charges $\hat{q}_j^z$ are analogous to the $\mathbb{Z}_2$ gauge field in the Kitaev model [52] and its ladder generalizations [57,58]. The presence of such local conserved charges is the hallmark of disorder-free localization [18–25].

We may then perform a two-site version of the Kramers-Wannier duality along the rungs of the ladder to dual spin-1/2 degrees of freedom $\hat{\eta}_j$ and $\hat{q}_j$: $\hat{X}_{1,j}\hat{X}_{2,j} \to \hat{\eta}_j^x$, $\hat{Z}_{1,j} \to \hat{\eta}_j^z$, and $\hat{Z}_{1,j}\hat{Z}_{2,j} \to \hat{q}_j^z$. In this language, the Hamiltonian (1) becomes

$$\hat{H}_{\text{Ising}} = -\Delta \sum_{j=1}^{L} \hat{\eta}_j^x - \sum_{j=1}^{L-1} (\Gamma_1 + \Gamma_2 \hat{q}_j^z \hat{q}_{j+1}^z)\hat{\eta}_j^z \hat{\eta}_{j+1}^z. \qquad (2)$$

There are three further equivalences to keep in mind. First, the transverse field Ising model (TFIM) (2) can be transformed, via a standard (leg-direction) Kramers-Wannier duality, to one in which the transverse field and interaction terms are interchanged. Second, either Ising model can be mapped to free fermions via a Jordan-Wigner transformation. Third, one can undo the (rung-direction) Kramers-Wannier duality to arrive at a plaquette-Ising model with the Hamiltonian

$$\hat{H}_{\square} = -\Delta \sum_{j} \hat{\sigma}_{1,j}^z \hat{\sigma}_{2,j}^z \hat{\sigma}_{1,j+1}^z \hat{\sigma}_{2,j+1}^z - \sum_{j,\alpha} \Gamma_\alpha \hat{\sigma}_{\alpha,j}^x. \qquad (3)$$

We will treat the disorder-free spin models (1), (3) as fundamental (for the purpose of identifying local physical observables). The full set of equivalent models is captured by Fig. 1.

Anderson localization.—The spectrum of Hamiltonian (2) can straightforwardly be constructed for any sector of the conserved charges $\{q_j\}$. For random $\{q_j\}$ (e.g., in high-temperature states), the dynamics is that of Majorana fermions with random binary hopping. The Hamiltonian (2) has an eigenstate phase transition [59–61] in a given sector of $\{q_j\}$ when $\langle \log|\Gamma_1 + \Gamma_2 q_j q_{j+1}|\rangle = \log|\Delta|$, where the average is over space. At infinite temperature, this transition point is at $|\Gamma_1^2 - \Gamma_2^2| = \Delta^2$. It separates a random paramagnet with localized excitations—for which the order parameter autocorrelation function, $\langle \hat{\eta}_i^z(t)\hat{\eta}_i^z(0)\rangle = \langle \hat{Z}_{1,i}(t)\hat{Z}_{1,i}(0)\rangle$, vanishes—from a "spin glass" phase, in which it does not. Note that, at the special value $\Gamma_1 = \Gamma_2$, the system is always paramagnetic, according to the criterion above. This follows because bonds for which $q_i q_{i+1} = -1$ are cut, and a finite segment of a system cannot undergo a phase transition. The phase transition separating these two dynamical phases is in the infinite-randomness universality class; at the transition point, the system is marginally localized with a localization length that diverges as the single particle energy vanishes $E \to 0$ [62].

As one lowers the temperature, the $\hat{q}_j^z$ become increasingly likely to align with their neighbors, so the localization length grows. At zero temperature, there is no randomness, and the system undergoes a ground-state phase transition that is in the Ising universality class. However, the

system is localized at any finite energy density above the ground state.

Entanglement growth.—Since the model (2) has free-fermion dynamics in any fixed sector, one can deduce that a general low-entanglement (e.g., product) initial state that is an eigenstate of all the $\hat{q}_j^z$ will quickly saturate to area law entanglement—at least away from the critical point for that sector. If we start, instead, from a superposition of $\hat{q}_j^z$ eigenstates, the entanglement exhibits unbounded slow logarithmic growth that is characteristic of MBL systems. This is our first main result, and in what follows, we intuitively explain why this happens and, then, explain how one can exploit the free-fermion character of the dynamics in each sector to efficiently compute the entanglement for relatively large systems.

One can imagine "integrating out" the free fermions to arrive at an effective classical spin model with Hamiltonian $\hat{H}_{\text{eff}}(\hat{q}_j^z)$. This Hamiltonian has diagonal interactions that decay exponentially in space with the characteristic fermionic localization length. Starting from an initial superposition, these interactions will cause slow dephasing, and, thence, slow entanglement growth, exactly as in Refs. [42–44]. One can illustrate this by considering a minimal example involving a 2×2 ladder. The Hamiltonian is $\hat{H}_{\text{toy}}=-(\Gamma_1+\Gamma_2\hat{q}_1^z\hat{q}_2^z)(\hat{c}_1^\dagger\hat{c}_2+\hat{c}_1^\dagger\hat{c}_2^\dagger+\text{H.c.})-\Delta\sum_j(1-2\hat{c}_j^\dagger\hat{c}_j)$. Considering, for simplicity, the sector with odd fermion parity (i.e., one fermion), the eigenstates have energies $\pm(\Gamma_1+\Gamma_2 q_1 q_2)$. Thus, if the initial state is a superposition of different $\hat{q}_j^z$ states, it will dephase on a time scale $\sim 1/\Gamma_2$ [63]. The dephasing rate between pairs of $\hat{q}_j$ falls off exponentially with distance, so at time t, each $\hat{q}_j$ is entangled with $\sim\xi\log(t/\xi)$ others [42].

Now, we consider, more generally, an initial product state of the compass spins $|\Psi\rangle=\hat{Z}_{1,j}|\Psi\rangle=\hat{X}_{2,j}|\Psi\rangle$. It can be written in terms of the Ising spins as

$$|\Psi\rangle=|\Phi\rangle\otimes\frac{1}{2^{L/2}}\sum_{q_j=\pm1}|\{q_j\}\rangle, \tag{4}$$

where $\hat{\eta}_j^z|\Phi\rangle=|\Phi\rangle,\ \forall\, j$. As a result, the product state (4) has an equal-weight projection onto every charge sector.

We bipartition the system legwise, into two ladders A and B, each of length $L_A=L_B=L/2$

$$\hat{\rho}_A(t)=\frac{1}{2^{L_A}}\sum_{\{\mu_j\}}\text{Tr}\left[\hat{\rho}(t)\prod_{j\in A}\hat{\eta}_j^{\mu_j}\right]\prod_{j\in A}\hat{\eta}_j^{\mu_j}, \tag{5}$$

where $\mu_j=0,1,2,3$, $\hat{\eta}_j^0$ is the identity and $\hat{\eta}_j^{1,2,3}=\hat{\eta}_j^{x,y,z}$. The Jordan-Wigner transformation maps the Hilbert space of the first L_A spins onto the first L_A fermions, and thus the density matrix of the spins and of the fermions is the same [64,65].

We find that, in terms of the $\hat{\eta}$ spins,

$$\text{Tr}\hat{\rho}_A^2=\frac{1}{2^{2L}}\sum_{\{q_1\},\{q_2\}}\text{Tr}_A[\text{Tr}_B\hat{U}(q_1^A,q_1^B)\hat{P}_\Phi\hat{U}^\dagger(q_2^A,q_1^B)\,\text{Tr}_B\hat{U}(q_2^A,q_2^B)\hat{P}_\Phi\hat{U}^\dagger(q_1^A,q_2^B)], \tag{6}$$

where $\hat{P}_\Phi=|\Phi\rangle\langle\Phi|$ is the projector onto the initial state of the $\hat{\eta}$ spins, and $\hat{U}(q^A,q^B)$ is the time evolution operator with a disorder configuration specified by $\{q\}=\{q^A\}\cup\{q^B\}$. The exponentiated Rényi entropy $e^{-S_2(t)}\propto\text{Tr}\hat{\rho}_A^2$ may be regarded as a disorder average over two independent charge configurations $\{q_1\}$ and $\{q_2\}$. The expression includes two forward time evolutions $\hat{U}(q^A,q^B)$, and two backward time evolutions $\hat{U}^\dagger(q^A,q^B)$, each containing a different Hamiltonian. However, the trace enforces that the disorder configurations appearing in these Hamiltonians are not independent. For the entropy $S_\alpha(t)$ with (integer) $\alpha>2$, there exist 2α replicas of the system with different disorder configurations correlated as per Eq. (6).

The expression (6) is evaluated numerically for $\alpha=2$ using the free-fermion techniques described in the Supplemental Material (SM) [66] and plotted in Fig. 2 for $\Gamma_2=\Delta=1$, and $\Gamma_1=1/2$ (with an average localization length $\xi\simeq 5.32$). After some initial transient dynamics, the growth of the entanglement entropy is seen to be logarithmic in time for sufficiently large systems, $S_2(t)\sim\xi\log(t/\xi)$, before finite size effects become relevant and the entropy saturates [73]. As shown in the inset, the late-time behavior of S_2 is volume law: $S_2(\infty)\propto L$.

We emphasize that the logarithmic entanglement growth is a consequence of the mixing between different q sectors in the Ising model; in a fixed q sector, the dynamics is described by an Ising model with binary disorder, for which entanglement growth saturates (away from the critical point). This is checked explicitly in the SM [66].

Dynamical structure factor.—Logarithmic entanglement growth, while central to the phenomenology of MBL systems, is not realistically measurable in most experiments. In what follows, we consider an observable that is straightforward to measure in solid-state experiments, which, we argue, also exhibits signatures of MBL that are related to the logarithmic growth. Let us consider the dynamical structure factor in the basis of the compass spins $\hat{\Sigma}_{\alpha,j}$, where $\hat{\Sigma}=\hat{X},\hat{Z}$. In particular, we are interested in the time dependence of $\langle\hat{\Sigma}_{\alpha,i}(t)\hat{\Sigma}'_{\beta,j}(0)\rangle$, where the angled brackets correspond to a finite temperature average with respect to the canonical ensemble. The trace over charge configurations $\{q_j\}$ implies that each $\hat{q}_j^\mu$ operator that projects out of a given sector must appear an even number of times for the expectation value to be nonvanishing. As a consequence, the mixed elements XZ and ZX must vanish identically.

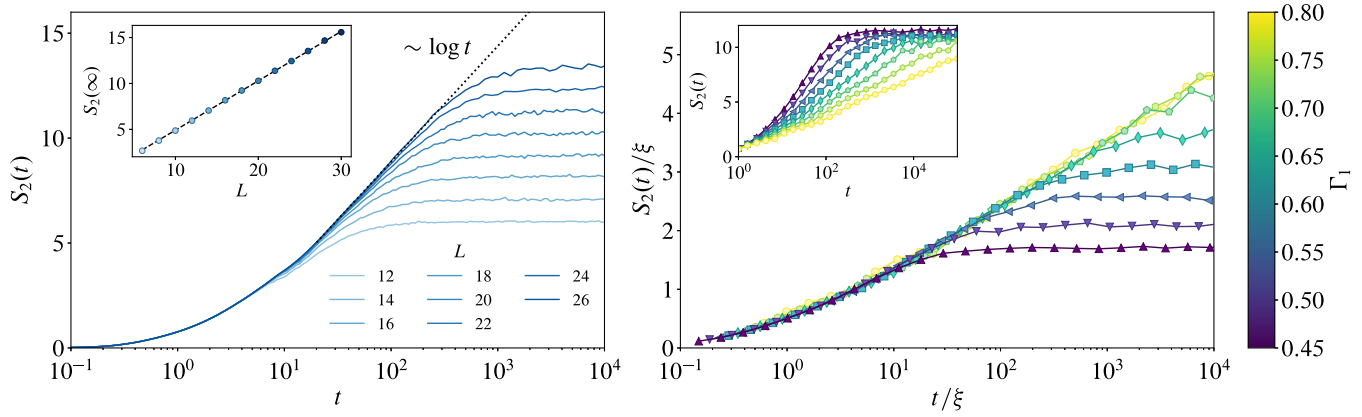

FIG. 2. Entanglement entropy $S_2(t)$ after beginning in the translationally invariant initial state (4) for a cut through the legs of the ladder that splits the system into two equal halves. Left panel: After some initial transient dynamics, $S_2(t)$ grows logarithmically in time, until it eventually saturates due to finite size. The saturation value is consistent with volume-law growth, as shown in the inset. Systems of size $L \leq 12$ ($N \leq 24$ spins) are calculated using exact diagonalization, while larger system sizes are evaluated using random sampling of Eq. (6) [74]. All curves are calculated using parameters $\Gamma_2 = \Delta = 1$, and $\Gamma_1 = 1/2$. Right panel: Scaling collapse of the data for a fixed system size $L = 22$ for various values of Γ_1, shown prior to rescaling in the inset, confirming the scaling $S_2(t) \sim \xi \log(t/\xi)$ that one may obtain within perturbation theory.

In the high-temperature limit, the nonzero components of the structure factor may be written as

$$\langle \hat{X}_{1,i}(t)\hat{X}_{1,j}(0)\rangle \propto \delta_{ij}\overline{\mathrm{Tr}[e^{i\hat{H}(\{q\})t}e^{-i\hat{H}_i^x(\{q\};-q_i)t}]}, \quad (7)$$

$$\langle \hat{Z}_{1,i}(t)\hat{Z}_{1,j}(0)\rangle \propto \delta_{ij}\overline{\mathrm{Tr}[e^{i\hat{H}(\{q\})t}e^{-i\hat{H}_i^z(\{q\})t}]}, \quad (8)$$

where the over line corresponds to an infinite-temperature average over the various charge sectors, $\hat{H}_i^\mu = \hat{\eta}_i^\mu \hat{H} \hat{\eta}_i^\mu$, and $\hat{H}(\{q\};-q_i)$ denotes that the sign of the spin q_i on site i has been flipped with respect to the configuration $\{q\}$ [75]. In both cases, the forward and backward Hamiltonians differ by some local perturbation in the real space spin basis and may be evaluated efficiently using free-fermion techniques [66].

Despite the apparent similarity between the two expressions, the behavior of the two components is markedly different. The reason for this difference is the absence (presence) of sector changing operators $\hat{q}_j^x$ in the ZZ (XX) correlator. The ZZ correlator, being diagonal in the conserved charges, maps directly onto the order parameter correlator of the Ising Hamiltonian in Eq. (2), $\langle \hat{\eta}_i^z(t)\hat{\eta}_j^z(0)\rangle$, for which only the autocorrelation function $i = j$ is nonzero at infinite temperature [76,77]. In the presence of emergent randomness, the behavior of this correlator can be understood in the excited-state real-space renormalization-group framework [60]. In the paramagnetic phase, this correlator decays to zero, while in the ferromagnet it saturates to a nonzero value. (In a finite system, the correlator eventually vanishes, but on a time scale that diverges with system size.) This plateau is shown in Fig. 3. Therefore, the ZZ correlator is not sensitive to the emergent nature of the disorder, and behaves identically to a TFIM in the presence of quenched disorder. That such behavior can occur in translationally invariant models is worthy of note but has been observed before in a variety of contexts (see, e.g., Refs. [18–25,58]).

Conversely, the XX correlator involves both flipping Ising spins and changing q sector. Since the forward and backward time evolutions involve different disorder

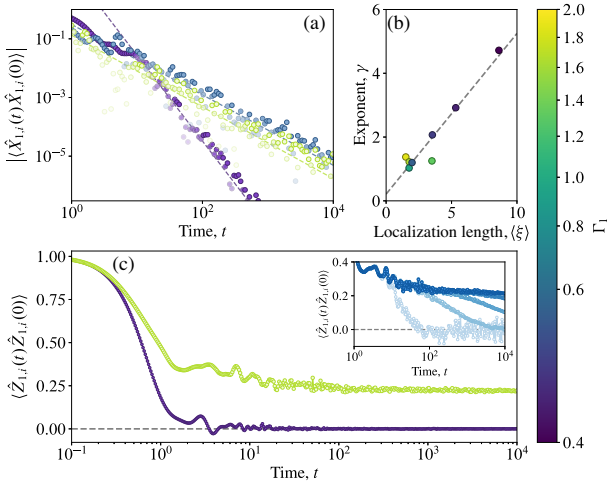

FIG. 3. Time dependence of the diagonal elements of the infinite-temperature dynamical structure factor in the compass spins, $\hat{X}_{\alpha,j}$ and $\hat{Z}_{\alpha,j}$, for $L = 48$ ($N = 96$ spins), and $\Gamma_2 = \Delta = 1$. (a) The XX correlator exhibits a decay consistent with Eq. (9): Power law $\sim t^{-\gamma}$, with an exponent proportional to the localization length ξ, as shown in panel (b). Conversely, the ZZ correlator (c) is diagonal in the conserved charges $\{\hat{q}_j^z\}$, and, hence, maps directly onto the corresponding spin correlation function of the disordered TFIM (2). The inset shows the divergence of the time scale over which the plateau decays with system size in the ferromagnetic phase (shown for $L = 8$, 16, 24, 32, 40).

realizations, the XX component is aware of the emergent character of the disorder. Therefore, the XX correlator exhibits phenomenology beyond that of conventional disordered systems and, by extension, beyond that of operators that are diagonal in the local conserved charges (distinguishing our results from, e.g., Ref. [58]). The differing forward and backward time evolutions imply that Eq. (7) is analogous to a Loschmidt echo after a local quench. Treating the difference between the forward and backward time evolutions as a perturbation $\sim\epsilon(\hat{\eta}^z_{i-1}\hat{\eta}^z_i + \hat{\eta}^z_i\hat{\eta}^z_{i+1})$ [78], we find that, in a typical q sector,

$$\langle \hat{X}_{1,i}(t)\hat{X}_{1,i}(0)\rangle \sim \prod_{n=1}^{L} \cos(\epsilon t[\psi^n_{i-1}\phi^n_i + \psi^n_i\phi^n_{i+1}]) \sim \left(\frac{\epsilon t}{\xi}\right)^{-c\xi}, \tag{9}$$

where the matrices ψ^n_j and ϕ^n_j diagonalize the fermionic Hamiltonian [79], and $c > 0$ is an $O(1)$ number. This correlation function is essentially the exponentiated entanglement, and represents our second main result. We see, in Fig. 3, that this power law decay is indeed seen in the numerics, with an exponent that is consistent with Eq. (9) (away from the critical point).

Discussion.—The central result of this Letter is that quasi-1D compass and plaquette Ising models, which arise naturally in various experimental settings [38], exhibit a form of disorder-free localization that bears many of the distinctive features of MBL. In particular, we have shown that the emergent character of the disorder—which permits superpositions of different disorder realizations and operators that modify the disorder configuration—can lead to the unbounded logarithmic growth of entanglement and anomalous power-law decay of correlation functions. This considerably broadens the scope of candidate materials for studying MBL and its dynamical signatures.

We established our results in a model that was solvable using free-fermion techniques; remarkably, the slow growth of entanglement, despite being inherently an interaction effect, is present in these free-fermion models because (as we explained here) integrating out the fermions gives rise to diagonal interactions and, thus, exponentially slow dephasing between distinct configurations of conserved variables. (Related phenomena had previously been found in out-of-time-order correlators [23,80].) As we argued, this slow dephasing also manifests itself in more experimentally accessible variables, such as the XX component of the dynamical structure factor. Note that, while logarithmic growth of entanglement is also seen in some other models with divergent localization lengths [81] or strong zero modes [80], the compass model in its paramagnetic phase exhibits neither of these features. Given the close parallels between the entanglement growth here and the physics of Loschmidt echoes for free fermions, the present model raises the prospect of deriving exact expressions for the asymptotics of entanglement and correlation functions, via solving a Riemann-Hilbert problem [82]; this is an interesting topic for future work.

A natural question our results raise is what happens for ladders with more than two legs? These systems still have one local conserved charge per rung (i.e., the product of $\hat{X}$ operators along the rung), which can generate emergent disorder, as in the two-leg case. They are, in general, strongly interacting and do not admit free-fermion solutions, and, thus, are beyond the scope of this Letter. For parameters where these models have an MBL phase, their phenomenology should resemble that studied here. However, such generic interacting models will also exhibit a delocalized thermal phase. How sector-changing operators like the XX correlator behave at the many-body delocalization transition remains an open question worthy of future consideration.

We would like to thank Pasquale Calabrese, Maurizio Fagotti, Max McGinley, Vadim Oganesyan, and Giuseppe De Tomasi for useful discussions. This work was supported in part by the Engineering and Physical Sciences Research Council (EPSRC) Grants No. EP/K028960/1, No. EP/M007065/1, and No. EP/P034616/1 (C. C. and O. H.). S. G. was supported in part by NSF Grant No. DMR-1653271. The simulations were performed using resources provided by the Cambridge Service for Data Driven Discovery (CSD3) operated by the University of Cambridge Research Computing Service (www.csd3.cam.ac.uk), provided by Dell EMC and Intel using Tier-2 funding from the Engineering and Physical Sciences Research Council (Capital Grant No. EP/P020259/1), and DiRAC funding from the Science and Technology Facilities Council (www.dirac.ac.uk).

[1] A. Polkovnikov, K. Sengupta, A. Silva, and M. Vengalattore, Rev. Mod. Phys. **83**, 863 (2011).
[2] C. Müller, J. H. Cole, and J. Lisenfeld, Rep. Prog. Phys. **82**, 124501 (2019).
[3] J. Maldacena, S. H. Shenker, and D. Stanford, J. High Energy Phys. 08 (2016) 106.
[4] D. Basko, I. Aleiner, and B. Altshuler, Ann. Phys. (N.Y.) **321**, 1126 (2006).
[5] R. Nandkishore and D. A. Huse, Annu. Rev. Condens. Matter Phys. **6**, 15 (2015).
[6] D. A. Abanin, E. Altman, I. Bloch, and M. Serbyn, Rev. Mod. Phys. **91**, 021001 (2019).
[7] S. Gopalakrishnan and S. Parameswaran, Phys. Rep. **862**, 1 (2020).
[8] J. Z. Imbrie, J. Stat. Phys. **163**, 998 (2016).
[9] Y. Kagan and L. Maksimov, Zh. Eksp. Teor. Fiz. **87**, 348 (1984).
[10] W. De Roeck and F. Huveneers, Commun. Math. Phys. **332**, 1017 (2014).
[11] M. Schiulaz and M. Müller, AIP Conf. Proc., **1610**, 11 (2014).

[12] M. van Horssen, E. Levi, and J. P. Garrahan, Phys. Rev. B **92**, 100305(R) (2015).
[13] Z. Papić, E. M. Stoudenmire, and D. A. Abanin, Ann. Phys. (Amsterdam) **362**, 714 (2015).
[14] N. Y. Yao, C. R. Laumann, J. I. Cirac, M. D. Lukin, and J. E. Moore, Phys. Rev. Lett. **117**, 240601 (2016).
[15] W. De Roeck and F. Huveneers, in *From Particle Systems to Partial Differential Equations II* (Springer, New York, 2015), pp. 173–192.
[16] W. De Roeck, F. Huveneers, M. Müller, and M. Schiulaz, Phys. Rev. B **93**, 014203 (2016).
[17] S. Gopalakrishnan and D. A. Huse, Phys. Rev. B **99**, 134305 (2019).
[18] A. Smith, J. Knolle, D. L. Kovrizhin, and R. Moessner, Phys. Rev. Lett. **118**, 266601 (2017).
[19] A. Smith, J. Knolle, R. Moessner, and D. L. Kovrizhin, Phys. Rev. Lett. **119**, 176601 (2017).
[20] A. Smith, J. Knolle, R. Moessner, and D. L. Kovrizhin, Phys. Rev. B **97**, 245137 (2018).
[21] M. Brenes, M. Dalmonte, M. Heyl, and A. Scardicchio, Phys. Rev. Lett. **120**, 030601 (2018).
[22] S. A. Parameswaran and S. Gopalakrishnan, Phys. Rev. Lett. **119**, 146601 (2017).
[23] A. Smith, J. Knolle, R. Moessner, and D. L. Kovrizhin, Phys. Rev. Lett. **123**, 086602 (2019).
[24] A. Russomanno, S. Notarnicola, F. M. Surace, R. Fazio, M. Dalmonte, and M. Heyl, Phys. Rev. Research **2**, 012003(R) (2020).
[25] P. Karpov, R. Verdel, Y. P. Huang, M. Schmitt, and M. Heyl, Phys. Rev. Lett. **126**, 130401 (2021).
[26] M. Schreiber, S. S. Hodgman, P. Bordia, H. P. Lüschen, M. H. Fischer, R. Vosk, E. Altman, U. Schneider, and I. Bloch, Science **349**, 842 (2015).
[27] S. S. Kondov, W. R. McGehee, W. Xu, and B. DeMarco, Phys. Rev. Lett. **114**, 083002 (2015).
[28] J.-y. Choi, S. Hild, J. Zeiher, P. Schauß, A. Rubio-Abadal, T. Yefsah, V. Khemani, D. A. Huse, I. Bloch, and C. Gross, Science **352**, 1547 (2016).
[29] P. Bordia, H. P. Lüschen, S. S. Hodgman, M. Schreiber, I. Bloch, and U. Schneider, Phys. Rev. Lett. **116**, 140401 (2016).
[30] J. Smith, A. Lee, P. Richerme, B. Neyenhuis, P. W. Hess, P. Hauke, M. Heyl, D. A. Huse, and C. Monroe, Nat. Phys. **12**, 907 (2016).
[31] A. Lukin, M. Rispoli, R. Schittko, M. E. Tai, A. M. Kaufman, S. Choi, V. Khemani, J. Léonard, and M. Greiner, Science **364**, 256 (2019), https://science.sciencemag.org/content/364/6437/256/tab-article-info.
[32] B. Chiaro *et al.*, arXiv:1910.06024.
[33] M. Ovadia, B. Sacépé, and D. Shahar, Phys. Rev. Lett. **102**, 176802 (2009).
[34] Z. Ovadyahu, Phys. Rev. Lett. **108**, 156602 (2012).
[35] Z. Ovadyahu, Phys. Rev. B **91**, 035113 (2015).
[36] M. Ovadia, D. Kalok, I. Tamir, S. Mitra, B. Sacépé, and D. Shahar, Sci. Rep. **5**, 13503 (2015).
[37] T. Nguyen, N. Andrejevic, H. C. Po, Y. Tsurimaki, N. C. Drucker, A. Alatas, E. E. Alp, B. M. Leu, A. Cunsolo, Y. Q. Cai *et al.*, arXiv:2008.02257.
[38] W. Brzezicki and A. M. Oleś, Phys. Rev. B **80**, 014405 (2009).
[39] M. Žnidarič, T. Prosen, and P. Prelovšek, Phys. Rev. B **77**, 064426 (2008).
[40] J. H. Bardarson, F. Pollmann, and J. E. Moore, Phys. Rev. Lett. **109**, 017202 (2012).
[41] R. Vosk and E. Altman, Phys. Rev. Lett. **112**, 217204 (2014).
[42] M. Serbyn, Z. Papić, and D. A. Abanin, Phys. Rev. Lett. **110**, 260601 (2013).
[43] M. Serbyn, Z. Papić, and D. A. Abanin, Phys. Rev. Lett. **111**, 127201 (2013).
[44] D. A. Huse, R. Nandkishore, and V. Oganesyan, Phys. Rev. B **90**, 174202 (2014).
[45] M. Serbyn, M. Knap, S. Gopalakrishnan, Z. Papić, N. Y. Yao, C. R. Laumann, D. A. Abanin, M. D. Lukin, and E. A. Demler, Phys. Rev. Lett. **113**, 147204 (2014).
[46] M. Serbyn, Z. Papić, and D. A. Abanin, Phys. Rev. B **90**, 174302 (2014).
[47] D.-L. Deng, X. Li, J. H. Pixley, Y.-L. Wu, and S. Das Sarma, Phys. Rev. B **95**, 024202 (2017).
[48] R. Vasseur, S. A. Parameswaran, and J. E. Moore, Phys. Rev. B **91**, 140202(R) (2015).
[49] S. Gopalakrishnan, M. Müller, V. Khemani, M. Knap, E. Demler, and D. A. Huse, Phys. Rev. B **92**, 104202 (2015).
[50] E. Dagotto, Rep. Prog. Phys. **62**, 1525 (1999).
[51] Z. Nussinov and J. van den Brink, Rev. Mod. Phys. **87**, 1 (2015).
[52] A. Kitaev, Ann. Phys. (Amsterdam) **321**, 2 (2006).
[53] L. M. Vasiloiu, F. Carollo, M. Marcuzzi, and J. P. Garrahan, Phys. Rev. B **100**, 024309 (2019).
[54] D. A. Johnston and R. P. Ranasinghe, Entropy **22**, 633 (2020).
[55] R. M. Nandkishore and M. Hermele, Annu. Rev. Condens. Matter Phys. **10**, 295 (2019).
[56] A. Prem, J. Haah, and R. Nandkishore, Phys. Rev. B **95**, 155133 (2017).
[57] X.-Y. Feng, G.-M. Zhang, and T. Xiang, Phys. Rev. Lett. **98**, 087204 (2007).
[58] A. Metavitsiadis and W. Brenig, Phys. Rev. B **96**, 041115 (R) (2017).
[59] D. A. Huse, R. Nandkishore, V. Oganesyan, A. Pal, and S. L. Sondhi, Phys. Rev. B **88**, 014206 (2013).
[60] D. Pekker, G. Refael, E. Altman, E. Demler, and V. Oganesyan, Phys. Rev. X **4**, 011052 (2014).
[61] J. A. Kjäll, J. H. Bardarson, and F. Pollmann, Phys. Rev. Lett. **113**, 107204 (2014).
[62] D. S. Fisher, Phys. Rev. B **51**, 6411 (1995).
[63] Dephasing occurs on a different time scale in the even parity sector where the eigenstates have energies $\pm\sqrt{(\Gamma_1+q_1q_2\Gamma_2)^2+4\Delta^2}$.
[64] M. Fagotti and P. Calabrese, J. Stat. Mech. (2010) P04016.
[65] Since the transformation that maps $\hat{\eta}$ to compass spins does not mix the A and B subsystems, the reduced density matrices of the $\hat{\eta}$ and compass spins are unitarily equivalent.
[66] See Supplemental Material at http://link.aps.org/supplemental/10.1103/PhysRevLett.126.227202 for (i) the free-fermion techniques employed in the calculation of the entanglement entropy and the correlation functions, (ii) the model's duality transformations, (iii) initial state dependence of the entanglement growth, and (iv) the growth of the von Neumann entanglement entropy, which includes Refs. [67–72].

[67] B. Kramer and A. MacKinnon, Rep. Prog. Phys. **56**, 1469 (1993).
[68] R. Sims and G. Stolz, Markov Proc. Relat. Fields **21**, 791 (2015).
[69] F. Monteiro, M. Tezuka, A. Altland, D. A. Huse, and T. Micklitz, arXiv:2012.07884.
[70] T. Rakovszky, F. Pollmann, and C. W. von Keyserlingk, Phys. Rev. Lett. **122**, 250602 (2019).
[71] Y. Huang, IOP SciNotes **1**, 035205 (2020).
[72] M. Žnidarič, Phys. Rev. B **97**, 214202 (2018).
[73] For simplicity, we focus on the second Rényi entropy, $S_2(t)$, but we expect the von Neumann entanglement entropy to exhibit similar logarithmic growth. See the Supplemental Material [66] for exact diagonalization results.
[74] Note that there exists a sign problem when performing this average. Consequently, an exponential number of disorder realizations in system size must be sampled to achieve convergence.
[75] The combined effect of commuting $\hat{\eta}_i^x$ and $\hat{q}_i^x$ through the Hamiltonian is to change $J_\pm = \Gamma_1 \pm \Gamma_2 \to -J_\mp$ on bonds i and $i-1$.
[76] E. Lieb, T. Schultz, and D. Mattis, Ann. Phys. (N.Y.) **16**, 407 (1961).
[77] J. Perk, H. Capel, G. Quispel, and F. Nijhoff, Physica (Amsterdam) **123A**, 1 (1984).
[78] S. Vardhan, G. De Tomasi, M. Heyl, E. J. Heller, and F. Pollmann, Phys. Rev. Lett. **119**, 016802 (2017).
[79] Specifically, the Majorana operators that diagonalize the fermionic Hamiltonian, $\hat{H} = \frac{i}{2}\sum_n \epsilon_n \hat{\lambda}_{2n-1}\hat{\lambda}_n$, are related to the real-space Majoranas via the transformations $\hat{a}_{2i} = \sum_n \psi_i^n \hat{\lambda}_{2n}$ and $\hat{a}_{2i-1} = \sum_n \phi_i^n \hat{\lambda}_{2n-1}$.
[80] M. McGinley, A. Nunnenkamp, and J. Knolle, Phys. Rev. Lett. **122**, 020603 (2019).
[81] G. De Tomasi, S. Roy, and S. Bera, Phys. Rev. B **94**, 144202 (2016).
[82] B. Braunecker, Phys. Rev. B **73**, 075122 (2006).